doi:10.1093/brain/awv089 BRAIN 2015: 138; 1583–1597 | 1583

BRAIN
A JOURNAL OF NEUROLOGY

The ependymal region of the adult human spinal cord differs from other species and shows ependymoma-like features

Daniel Garcia-Ovejero,[1] Angel Arevalo-Martin,[1] Beatriz Paniagua-Torija,[1] José Florensa-Vila,[2] Isidro Ferrer,[3] Lukas Grassner[4,5] and Eduardo Molina-Holgado[1]

Several laboratories have described the existence of undifferentiated precursor cells that may act like stem cells in the ependyma of the rodent spinal cord. However, there are reports showing that this region is occluded and disassembled in humans after the second decade of life, although this has been largely ignored or interpreted as a post-mortem artefact. To gain insight into the patency, actual structure, and molecular properties of the adult human spinal cord ependymal region, we followed three approaches: (i) with MRI, we estimated the central canal patency in 59 control subjects, 99 patients with traumatic spinal cord injury, and 26 patients with non-traumatic spinal cord injuries. We observed that the central canal is absent from the vast majority of individuals beyond the age of 18 years, gender-independently, throughout the entire length of the spinal cord, both in healthy controls and after injury; (ii) with histology and immunohistochemistry, we describe morphological properties of the non-lesioned ependymal region, which showed the presence of perivascular pseudorosettes, a common feature of ependymoma; and (iii) with laser capture microdissection, followed by TaqMan® low density arrays, we studied the gene expression profile of the ependymal region and found that it is mainly enriched in genes compatible with a low grade or quiescent ependymoma (53 genes); this region is enriched only in 14 genes related to neurogenic niches. In summary, we demonstrate here that the central canal is mainly absent in the adult human spinal cord and is replaced by a structure morphologically and molecularly different from that described for rodents and other primates. The presented data suggest that the ependymal region is more likely to be reminiscent of a low-grade ependymoma. Therefore, a direct translation to adult human patients of an eventual therapeutic potential of this region based on animal models should be approached with caution.

1 Laboratory of Neuroinflammation, Hospital Nacional de Paraplejicos (SESCAM), Toledo, Spain
2 Radiology Unit, Hospital Nacional de Paraplejicos (SESCAM), Toledo, Spain
3 Institut de Neuropatologia, Servei d'Anatomia Patolo'gica, IDIBELL-Hospital Universitari de Bellvitge, L'Hospitalet de Llobregat, Spain
4 Center for Spinal Cord Injuries, Trauma Center Murnau, Germany
5 Institute of Molecular Regenerative Medicine, SCI-TReCS (Spinal Cord Injury and Tissue Regeneration Center Salzburg), Paracelsus Medical University, Salzburg, Austria

Correspondence to: Daniel Garcia-Ovejero,
Laboratory of Neuroinflammation,
Hospital Nacional de Paraplejicos,
Finca La Peraleda s/*n*, 45071-Toledo,
Spain
E-mail: dgarciao@sescam.jccm.es

Keywords: neural stem cells; spinal cord injury; ependymoma; regeneration; central canal

Abbreviations: AUC = area under the curve; GLAST = glutamate aspartate transporter; SCI = spinal cord injury

Received November 4, 2014. Revised January 20, 2015. Accepted January 30, 2015. Advance Access publication April 15, 2015

Introduction

Replacement of dead and damaged cells may be a promising strategy to restore function after damage to the spinal cord (Abematsu *et al.*, 2010; Tetzlaff *et al.*, 2011; Lu *et al.*, 2014); this might be achieved by activating endogenous sources of new cells (Weiss *et al.*, 1996; Johansson *et al.*, 1999; Yang, 2006; Barnabé-Heider *et al.*, 2010). In recent years, a neurogenic region in the adult rodent and primate spinal cord has been described, which is formed by cells surrounding the central canal that proliferate and generate a variety of cell types *in vivo* and behave like neural stem cells *in vitro* (Weiss *et al.*, 1996; Shihabuddin *et al.*, 1997; Johansson *et al.*, 1999; Horner *et al.*, 2000; Yamamoto *et al.*, 2001; Dromard *et al.*, 2008; Meletis *et al.*, 2008; Sabourin *et al.*, 2009; Barnabé-Heider *et al.*, 2010; Alfaro-Cervello *et al.*, 2012).

Most of the studies regarding the human ependymal region have been performed on children or very young individuals, where the central canal is patent, showing a structure and cell composition with some particularities, but largely similar to that described for mice, rats and macaques (Koelliker, 1893; Retzius, 1893; von Lenhossek, 1895; Ramon y Cajal, 1899/1904; Sakakibara *et al.*, 2007; Dromard *et al.*, 2008; Hugnot and Franzen, 2011; Alfaro-Cervello *et al.*, 2014). However, a few studies report a completely different pattern in the adult human spinal cord: there is an almost complete absence of a patent central canal in the whole cord from the second decade of life (Clarke, 1859; Weigert, 1895; Cornil, 1933; Netsky, 1953; Kasantikul *et al.*, 1979; Milhorat *et al.*, 1994; Yasui *et al.*, 1999). The former canal is replaced by a disassembled and morphologically heterogeneous accumulation of cells, composed mainly of astrocyte gliosis, ependymocytes, and small cellular arrangements described as rosettes or pseudocanals (Kasantikul *et al.*, 1979; Milhorat *et al.*, 1994; Yasui *et al.*, 1999; Hugnot and Franzen, 2011; Alfaro-Cervello *et al.*, 2014). Those descriptions have not pervaded the field and it has been proposed that obliteration could be an artefact due to post-mortem tissue processing (Dromard *et al.*, 2008). As a consequence, the rationale for clinical translation is still based on rodent models (Goritz and Frisen, 2012; McDonough and Martinez-Cerdeno, 2012; Sabelstrom *et al.*, 2014).

In the current work, we performed a systematic study of the spinal cord ependymal region in adult humans, using three different approaches: (i) using MRI, we studied central canal patency in healthy volunteers and in patients with traumatic and non-traumatic spinal cord injury (SCI) to establish the proportion of central canal stenosis that is normal or due to a post-mortem artefact; (ii) with histology and immunohistochemistry, we characterized the morphology of the adult human ependymal region; and (iii) using laser capture microdissection followed by real time PCR, we explored the molecular properties of cells forming that region to determine whether their gene expression profile was compatible with a neural stem cell niche.

Materials and methods

MRI

Healthy volunteers

We recruited 59 healthy volunteers of different ages, without any pre-existing spinal cord pathology. Age and sex distribution are shown in Supplementary Table 1. We acquired T_2-weighted images of the entire spinal cord of each volunteer in axial, sagittal and horizontal planes, from C1 to the conus medullaris, using a MRI 3 T Trio Tim (Siemens) at the Radiology Service in the National Hospital for Paraplegics. The MRI sequences used are described in the Supplementary material. Axial planes were acquired every 2 mm. Horizontal and sagittal planes were acquired with no gap between planes.

All patients enrolled signed consent for MRI acquisition. Data procurement and handling were carried out in accordance with the Spanish law (LOPD 15/1999; RD 1720/2007). The study protocol followed the International Health Guidelines (Declaration of Helsinki, 2008) and received approval by the Clinical Investigation Ethical Committee (CEIC) at our institution.

Visual scoring of canal patency

After a first evaluation of MRI images (blinded to the age and sex of each volunteer), we established three categories of central canal based on the patency observed: (i) a patent central canal; (ii) a partially patent canal; and (iii) an absent canal (Fig. 1A–D). A patent central canal was defined as a strong hyperintense round signal in the midpoint of the central grey matter region, showing no continuity with the ventral sulcus. This last criterion was required to avoid misinterpretations due to the hyperintense signal that is frequently observed in the region of the anterior median fissure.

A partially patent/absent canal was defined as a medium/low hyperintense round signal located in the midpoint central grey region, showing no continuity with the ventral sulculs. This type of canal is smaller in diameter than the patent type and hyperintensity is much lower, but it is still clearly distinguishable from the rest of the normo-intense parenchyma.

An absent canal was defined in the rest of the cases. This included the vast majority of levels showing normo-intensity in the whole cross-section of the cord and also some levels showing a diffuse signal with a very low hyperintensity in the central grey region, difficult to distinguish from other normal low hyperintensities present in the spinal cord. We scored images with restrictive criteria, which indicates that in case of doubt, the lower patency score was given to that particular image.

Quantitative scoring of canal patency

To rule out a subjective bias in the scoring and also to allow us to perform mathematical comparisons in advance, an additional quantitative estimation of canal patency was performed on each image in the axial plane. Images were zoomed to view in greater detail an area including the spine and spinal cord (50 mm × 50 mm). This region was exported in high resolution (final resolution 17 pixel/mm) and then loaded in ImageJ.

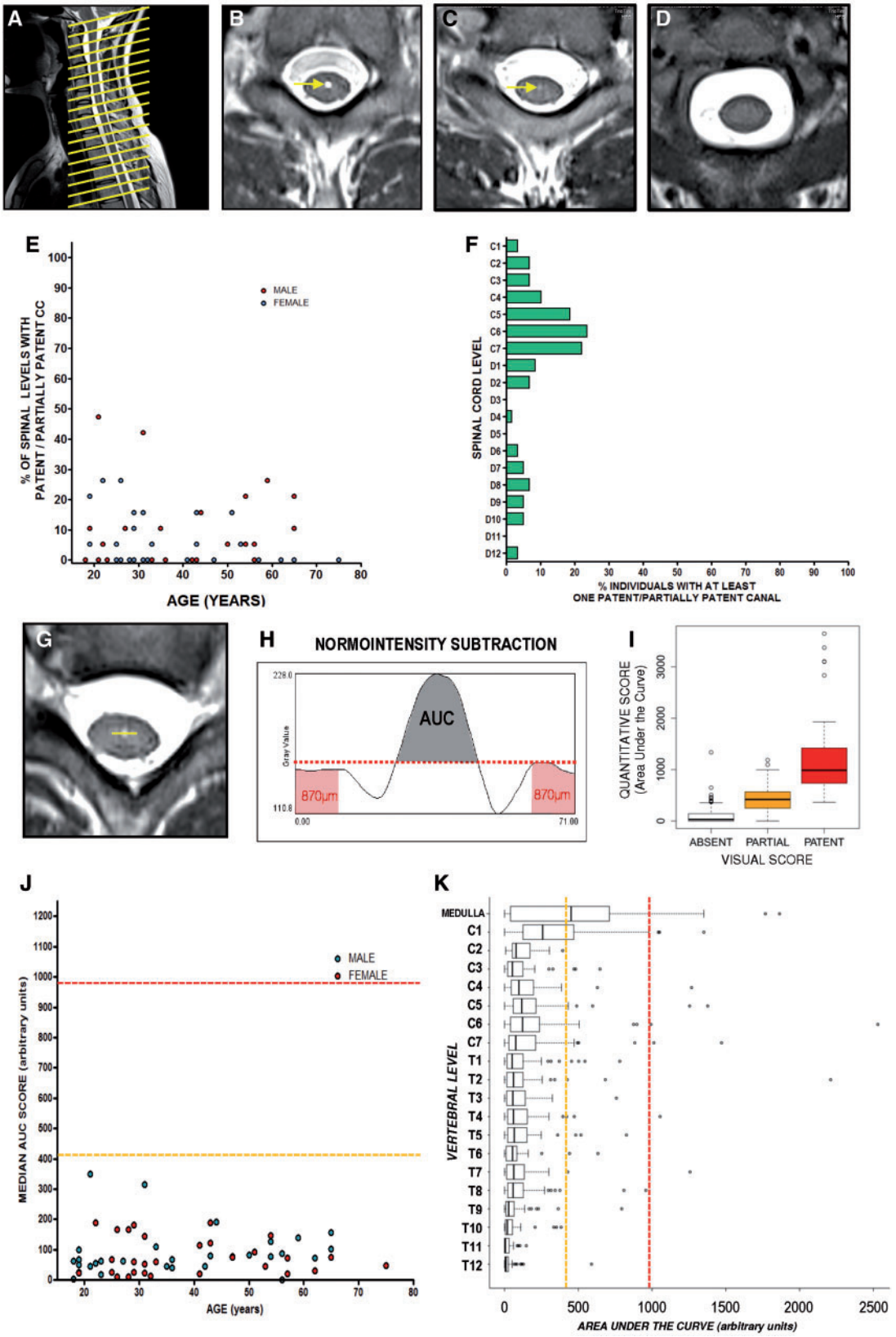

Figure 1 Estimation of central canal patency in healthy volunteers by T_2-weighted MRI. (**A**) Sagittal image showing the acquisition of axial planes in the spinal cord of volunteers. (**B**) Axial plane showing a representative level with a patent central canal (*arrow*). (**C**) Axial plane showing a representative level of a partially patent canal (*arrow*). (**D**) Axial plane showing a representative level with absence of central canal. (**E**) Representation of the ratio of spinal levels with a patent or partially patent central canal in each individual based on visual scoring. (**F**) Representation of the proportion of individuals with patent or partially patent canal at a specific spinal cord level obtained with the visual score.

(continued)

Using the line drawing tool, a 4.18-mm long line was placed on the central grey matter so that the midpoint of the line was located in the middle of the hyperintense signal belonging to the central canal or in the centre of central grey corresponding to the location where the central canal was expected to be in the images when no hyperintensity was observed (Fig. 1H). Then, we subtracted 'normo-intensity' from the whole profile, defining normo-intensity as the maximum grey value in the outer edges of the line (0.87 mm each side) that fell on grey matter outside the central canal region (Fig. 1H). After subtraction, the area under the curve (AUC) of the resulting new profile (hyperintensity profile) was considered to be the quantitative estimation of canal patency (Fig. 1G and H).

AUC scores obtained with this method closely correlated with our visual scoring (Fig. 1I): median AUC score for patent canals = 986; median AUC score for partially patent canals = 418.98; median AUC score for absent canals = 28.34. We performed an additional validation of the quantification method using rat spinal cords (consistent central canal patency along the whole extension of the cord), which is detailed in Supplementary Fig. 1.

Injured patients

Images from injured patients were obtained from the databases of the National Hospital for Paraplegics (HNP; Toledo, Spain) and from the Center for Spinal Cord Injuries at the Trauma Center Murnau (TCM; Germany). Data corresponding to the lesion level, age of the patient at lesion, age of the patient at MRI, sex, ASIA evaluation at the according time point of MRI acquisition, and diagnostic measurements were recorded for each patient. Patient data procurement and handling were carried out in accordance with the published International Health Guidelines (Declaration of Helsinki, 2008) and the Spanish law (LOPD 15/1999; RD 1720/2007). Based on their clinical diagnosis we subdivided patients into two categories: traumatic and non-traumatic spinal cord injuries. The latter category was then subdivided according to the different origins of the damage: ischaemic or vascular origin, damage due to infections or myelitis, demyelinating diseases and tumours. Images from the HNP were all acquired with a 3 T Trio Siemens machine, whereas images at MTC were obtained with either a 1.5 T Philips Achieva or a 3 T Philips Achieva machine. Multiple linear regression and covariate analysis of AUCs obtained from the different machines showed no significant difference in scores in relation to the machine used. Therefore, the rest of the analysis included all patients, irrespective of their origin.

Distribution and characteristics of traumatic SCI patients ($n = 99$) are shown in Supplementary Table 2. Briefly, the vast majority were males (81 males versus 16 females), patients ranged from 18 to 77 years old at the moment of lesion (median = 34.13; mean = 39.41), and they included an extended interval of post-lesion times: from the same lesion day (Day 0) to more than 40 years (Day 15 212). Non-traumatic SCI patient numbers were much lower: ischaemic or vascular origin ($n = 4$), damage due to infections or myelitis ($n = 13$), demyelinating diseases ($n = 3$) and tumours ($n = 6$).

We used the method described above to quantify patency scores. In the case of traumatic SCI patients, we measured three different scores after excluding regions in which central grey matter was disrupted, as the primary focus of the lesion (Fig. 2A–E): for the first score, we obtained the median AUC patency score of unlesioned levels, i.e. levels without perceivable disturbances of T_2 signal; for the second score, we obtained the median AUC patency score of lesioned levels, i.e. showing T_2 signal disturbances not affecting central grey matter; and for the third score, we obtained the median AUC patency score of levels adjacent to the main focus of the lesion focus (~3–4 mm rostral and caudal). For non-traumatic patients, only two scores are shown: unlesioned levels score, and lesioned levels score, because no primary focus is normally observed that would allow us to define the adjacent levels score.

Data analysis

After observing that both raw and log-transformed data were not normally distributed (Shapiro test), we used robust estimators and hypothesis testing to compare groups (Mann-Whitney U-test or Kruskal-Wallis test followed by Dunn post-tests) and to study associations between variables (Spearman correlations). These tests (including non-supervised hierarchical clustering, Supplementary Fig. 2) were performed using Graph Pad Prism 5.0 software and R (R Development Core Team, 2014). The use of these tests is specified for each experiment in the 'Results' section.

Histology and immunohistochemistry

Source of the samples

Human tissue was obtained from two public tissue biobanks: the HUFA BioBank (Biobanco del Hospital Universitario Fundación Alcorcón, Alcorcon, Spain) and the Neurological Tissue Bank (Banco de Tejidos Neurológicos, IDIBELL-Hospital Universitario de Bellvitge, Hospitalet de Llobregat, Barcelona, Spain). Tissue was provided in 5–8 mm thick

Figure 1 Continued

(**G** and **H**) Schemes depicting the protocol of quantification of central canal patency using ImageJ. (**G**) A line is drawn in the central grey with the centre in the coordinate corresponding to the expected position of central canal. (**H**) After obtaining grey intensity profile, normo-intensity is subtracted using the maximum grey intensity value in the external parts of the region of interest (red area), and area under the resultant curve (AUC, shaded region) is used as estimation of central canal patency. (**I**) A good equivalence is found between visual and quantitative scores. (**J**) Representation of median value (general score) of each individual shows a general absence of central canal patency in adult humans. Median values obtained from partially patent canals (dashed orange line) or patent canals (dashed red line) are shown as a reference. (**K**) Distribution of quantitative scores throughout the spinal levels of all individuals. Scores are far from the levels of patency (dashed red line) and partial patency (dashed orange line) except for low medulla and cervical level 1, where half and a quarter of individuals, respectively, present a score compatible with at least partial patency.

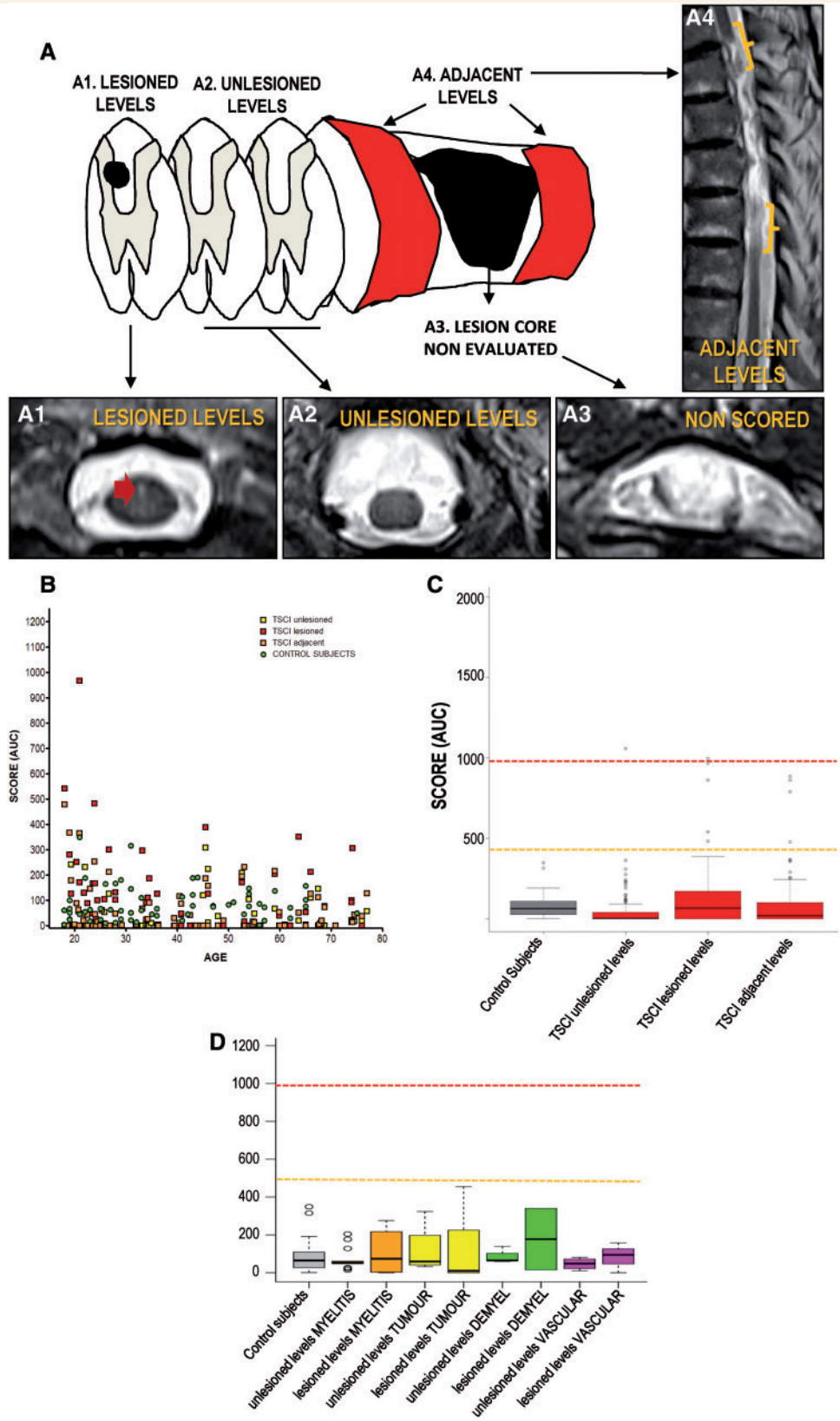

Figure 2 Estimation of central canal patency in patients with spinal cord injury by T_2-weighted MRI. (**A**) Scheme depicting the acquisition of axial planes in the spinal cord of injured patients. Adapted from Beattie (2004). (**A_1**) Axial plane showing a representative image of planes used to establish the 'lesioned levels' score. Red arrow points to a hyperintense lesion located outside the central grey matter. (**A_2**) Axial plane showing a representative image of planes used to establish the 'unlesioned levels' score. (**A_3**) Axial plane showing a representative image of the region excluded from analysis. (**A_4**) Sagittal plane showing regions (brackets) used to establish the 'adjacent levels' score.

(continued)

formalin fixed blocks. Samples were obtained from nine deceased individuals without clinical or histopathological involvement of the spinal cord (Table 1). Upon receipt, tissue blocks were embedded in low melting agarose with 10% sucrose in 0.1 M phosphate-buffered saline (PBS) and cut into serial transverse sections (40 µm) with a vibrating microtome (Leica VT 1000 M). Sections were then stored at −18 °C in Olmos solution until use.

Histology and immunohistochemistry

Immunohistochemistry was performed on sections rinsed in rinse solution containing 0.1 M PBS (pH 7.4) and 0.5% bovine serum albumin (BSA). Endogenous peroxidase activity was inhibited by incubating the sections in 0.1 M PBS containing 1.8% H_2O_2 and 50% methanol; sections were extensively rinsed with rinse solution plus 0.1% Triton™ X-100. The sections were then subjected to antigen demasking, consisting of a 30 min pretreatment with a 0.05% solution of citraconic anhydride (Sigma, #27430) at 96 °C, followed by temperature re-accommodation at room temperature for at least 30 additional minutes (Namimatsu *et al.*, 2005; Alelu-Paz *et al.*, 2008). After extensive rinse solution rinsing, sections were incubated for 2 nights with the primary antibodies detailed in Supplementary Table 3, carefully rinsed and incubated for 2 h at room temperature with a horseradish peroxidase (HRP)-conjugated secondary antibody (1:300); they were developed with a solution of 0.03% diaminobenzidine and 0.01% hydrogen peroxide in 0.1 M PBS. Sections were analysed with a Leica DMR microscope.

A similar protocol was used for multiple labelling studies, although in this case the primary antibodies were detected using fluorophore-conjugated antibodies (Supplementary Table 4). Sections were mounted with Immumount (Thermo Scientific) and analysed with a LEICA SP5 confocal microscope at the Microscopy Facility in the National Hospital for Paraplegics (Toledo, SESCAM). Images were transferred to ImageJ (NIH, Bethesda, MD) and Adobe Photoshop (San Jose, CA) for cropping; they were adjusted to optimize contrast and brightness. Noise was reduced using a median filter with Fiji (http://pacific.mpi-cbg.de), a scientific image processing application based on ImageJ (http://rsb.info.nih.gov/ij). Semi-thin sections and electron microscopy were performed as described in the Supplementary material.

Gene expression in human ependymal region

Laser capture microdissection

Fresh frozen spinal cord blocks (5 mm thick) were provided by the Neurological Tissue Bank (Banco de Tejidos Neurológicos, IDIBELL-Hospital Universitario de Bellvitge, Hospitalet de Llobregat, Barcelona, Spain). All procedures were performed in RNase-free conditions. Frozen blocks were cut into 25-µm thick sections with a Leica CM1850 cryostat, and collected on PEN-Membrane slides (Leica #11505158). Slides were quickly stained with Toluidine blue (Supplementary material) to identify accumulations of cell nuclei in the centre of lamina X, corresponding to the ependymal region. We carefully microdissected those cells with a LMD 6000 Leica Dissection Microscope (Fig. 4A). Microdissected pieces were collected on RNA extraction buffer, and RNA extracted according to the manufacturer's instructions (Arcturus PicoPure® RNA Isolation Kit, Applied Biosystems). Evaluation of RNA integrity, purity and concentration was assessed with chip-based automated electrophoresis performed with the Experion™

Table 1 Post-mortem spinal cord tissue samples used for histology

Autopsy number	Cause of death	Gender	Age	Coded as	Post-mortem delay
BC01015	Unknown. No significant neuropathological alterations in the spinal cord	Male	60	Control	Unknown
BC00582	Unknown. No significant neuropathological alterations in the spinal cord	Male	21	Control	Unknown
BC01684	Acute hypoxia-ischaemia	Male	27	Control	Unknown
A07/00044	Cardiopulmonary arrest	Male	39	Control	3 h 30 min
A07/00041	Multiorganic failure. Gastric tumour	Male	43	Control	5 h 55 min
A07/00084	Refractary septic shock	Male	46	Control	15 h
A07/00067	Refractary septic shock and cardiac arrest. Ischaemic cardiopathy	Male	47	Control	4 h 55 min
A10/00017	Hepatic metastasis. Probable pancreatic neoplasia	Male	52	Control	3 h
A10/00026	Multiorganic failure. Severe broncopathy	Male	61	Control	3 h 55 min
B13-1146A	Glioblastome	Female	73	Tumour	
B13- 5651C	Astrocytome	Male	42	Tumour	

Figure 2 Continued

(**B**) Distribution of the three quantitative scores measured after traumatic SCI. A general absence of central canal patency is observed, and the scores of SCI individuals are intermingled with those found in healthy controls (green). Dots represent the median value (general score) of each individual. (**C**) Comparison between the scores found in healthy controls and patients with traumatic SCI. No significant increases are found after injury. Reference lines are shown for the values corresponding to partially patent canals (orange) or patent canals (red). (**D**) Comparison between healthy volunteers and scores found in patients with non-traumatic injuries. Again, no significant increase is found in any of the scores of any of the different conditions.

Table 2 Post-mortem spinal cord tissue samples used for laser capture microdissection.

Autopsy number	Cause of death	Gender	Age	Coded as	Post-mortem delay
A07/00084	Refractary septic shock	Male	46	Control	15 h
A10/00026	Multiorganic failure. Severe broncopathy	Male	61	Control	3 h 55 min
A05/00134	Carcinoma and metastasis. With brain but not spinal cord metastasis.	Female	32	Control	11 h 45 m
A11/00052	Endocarditis. No neuropathological features	Male	76	Control	6 h 30 m
A12/00046	Cardiac arrest. No neuropathological features	Female	75	Control	6 h 10 m

RNA HighSens Analysis Kit (Bio-Rad). Ependyma (n = 30–70) were collected per individual; 15–150 ng of total RNA was obtained. We also collected microdissected portions of ventral grey matter from each individual, which we used as a non-neurogenic, non-ependymal reference for gene expression.

mRNA amplification

A two-round amplification was performed with the ExpressArt® TRinucleotide mRNA Amplification Kit (#6299-A15, AmpTec, AMSBIO) (Hu *et al.*, 2008), according to the manufacturer's instructions. This kit was developed for amplification of mRNAs or mRNA fragments without poly(A) and for severely degraded eukaryotic RNAs (Hu *et al.*, 2008). More details about this procedure are provided in the Supplementary material. After amplification, mRNA concentration and purity was assessed by electrophoresis (Bio-Rad Experion™ StdSens kit) and by spectrophotometry (Nanodrop, Thermo Scientific). We amplified 3.7–37 ng of total RNA, obtaining between 6 and 21 µg of mRNA after two rounds. After collecting samples and studying the RNA integrity and quantity, samples from five different individuals who showed the best integrity scores were selected for gene expression assays (Table 2). We were able to microdissect both ependymal and ventral horn region from three of them, but only ependymal region from Patient A12/00046, and only ventral horn from Patient A11/00052. This rendered a final sample size of four ependymal regions and four ventral horns for gene expression assays.

Gene expression assays

Using cDNA from the ependymal region obtained by laser capture microdissection (LCMD), we tested whether the gene expression profile of those cells was compatible with either (i) a stem cell niche; or (ii) ependymoma. To this end, we designed two different TaqMan® low density arrays (TLDAs; Life Technologies) including two different panels of genes. The first panel (stemness panel, Table 3 and Supplementary Table 5) included 94 genes reported as present in the spinal cord central canal by studies carried out in rats, mice, primates and humans, plus other genes typically found in neurogenic niches (Johansson *et al.*, 1999; Yamamoto *et al.*, 2001; Fu *et al.*, 2003; Dromard *et al.*, 2008; Meletis *et al.*, 2008; Ceruti *et al.*, 2009; Kelly *et al.*, 2009; Sabourin *et al.*, 2009; Obermair *et al.*, 2010; Hugnot and Franzen, 2011; Petit *et al.*, 2011; Pfenninger *et al.*, 2011; Tysseling *et al.*, 2011; Alfaro-Cervello *et al.*, 2012, 2014; Fandel *et al.*, 2013; Mamber *et al.*, 2013; Sabelstrom *et al.*, 2014). The second panel of genes (ependymoma panel; Table 4 and Supplementary Table 6) included 94 genes from reports studying spinal, infratentorial, and posterior fossa ependymomas (Taylor *et al.*, 2005; Modena *et al.*, 2006; Palm *et al.*, 2009; Puget *et al.*, 2009; Andreiuolo *et al.*, 2010; Carro *et al.*, 2010; Johnson *et al.*, 2010; Peyre *et al.*, 2010; Witt *et al.*, 2011; Milde *et al.*, 2012; Wani *et al.*, 2012; Parker *et al.*, 2014). Based on our preliminary tests and manufacturer technical recommendations for TaqMan® assays, we chose 18S gene as an endogenous control, as it showed higher reproducibility and lower variation between samples than other reference genes (*GADPH*, *ACTB*).

Table 3 Expression of genes related to stem cell niches enriched in adult human ependymal region

Gene	Assay	Expressed only in ependymal region	Enriched in ependymal region*
BDNF	*Hs02718934_s1*	+	-
CD24	*Hs03044178_g1*	–	28.99
FOXJ1	*Hs00230964_m1*	–	169.59
MSI1	*Hs00159291_m1*	–	447.37
PAX6	*Hs00240871_m1*	–	463.99
PAX7	*Hs00242962_m1*	–	22.32

*Statistically significant expression versus ventral horn (Student t-test, $P < 0.05$). Numbers represent folds of enrichment (relative quantity) between gene expression in ependymal region and ventral horn.

Reverse transcription of amplified RNA was performed with ExpressArt® TR cDNA synthesis kit (#8994-A30, AmpTec, AMSBIO). We then added 60 ng of our samples pre-mixed with TaqMan® Universal Master Mix II (Life Technologies) into each loading port of the TLDA (1.25 ng cDNA/well). Cards were then centrifuged and run on an Applied Biosystems® 7900HT Fast Real-Time PCR System.

We aimed to diminish the possibility of false-negative results in genes that were not detected across samples. For those genes, we performed a second TaqMan® gene expression assay with primers and probes directed against a different region of the gene (see extra assay column in Supplementary Tables 5 and 6).

Data analysis

Automatic detection of cycle threshold (Ct) was used to establish the threshold of amplification for each gene. After averaging cycle thresholds from technical duplicates, we calculated ΔCt, the difference between the cycle threshold of each gene and the cycle threshold of the endogenous gene (18S) for that sample. Genes expressed in at least three out of four samples

Table 4 Expression of genes related to ependymoma in adult human ependymal region

Gene	Assay	Expressed only in ependymal region	Enriched in ependymal region*
AGBL2	*Hs00227128_m1*	+	–
ARHGEF28	*Hs00223736_m1*	+	–
ATP4B	*Hs01026288_m1*	+	–
C9orf24	*Hs00375666_m1*	+	–
CD47	*Hs00179953_m1*	+	–
CFTR	*Hs00357011_m1*	+	–
CYP11A1	*Hs00167984_m1*	+	–
DIRAS3	*Hs02330364_s1*	+	–
EFHB	*Hs01001334_m1*	+	–
EFNB3	*Hs00154861_m1*	+	–
FREM1	*Hs00381549_m1*	+	–
IGF1	*Hs01547656_m1*	+	–
IL5RA	*Hs00602482_m1*	+	–
MAL2	*Hs00294541_m1*	+	–
MATN2	*Hs00242753_m1*	+	–
NELL2	*Hs00196254_m1*	+	–
PON3	*Hs01023629_m1*	+	–
ROPN1L	*Hs00230481_m1*	+	–
SCN1A	*Hs00374696_m1*	+	–
SCN9A	*Hs00161567_m1*	+	–
C2orf40	*Hs00260897_m1*	–	2660.17
CCDC33	*Hs00228113_m1*	–	130 332
CHEK2	*Hs00200485_m1*	–	57 846.7
CXXC4	*Hs00228693_m1*	–	24 525.7
FHL1	*Hs00793641_g1*	–	16 829.3
HEY2	*Hs00232622_m1*	–	3267.27
HOXA5	*Hs00430330_m1*	–	21 721.7
HOXA7	*Hs00600844_m1*	–	916.45
HOXC10	*Hs00213579_m1*	–	797.32
HOXC8	*Hs00224073_m1*	–	1503.2
HOXC9	*Hs00396786_m1*	–	2745.81
INHBA	*Hs01081598_m1*	–	12 353.7
INPP5D	*Hs00183290_m1*	–	150.05
KLHDC8A	*Hs01000616_m1*	–	6242.35
LEPREL1	*Hs00216998_m1*	–	5074.82
LINGO2	*Hs01102041_s1*	–	916.22
LRRC2	*Hs00225885_m1*	–	32 362.03
MNS1	*Hs00218032_m1*	–	438 099.512
MPDZ	*Hs00187106_m1*	–	2909.56
NR4A3	*Hs00545009_g1*	–	322.52
PGAM2	*Hs00165474_m1*	–	121.29
RELN	*Hs01022646_m1*	–	7196.45
RXRG	*Hs00199455_m1*	–	11 208.13
SEMA3A	*Hs00173810_m1*	–	6755.72
SLIT3	*Hs00171524_m1*	–	20.33
SORBS1	*Hs00908953_m1*	–	22.02
TGFBR3	*Hs01114253_m1*	–	1324.2
TSGA10	*Hs00228873_m1*	–	25 688.26
WDR96	*Hs00401723_m1*	–	91 897.35
ZBTB18	*Hs00295755_s1*	–	111.66

*Statistically significant expression versus ventral horn (Student *t*-test, $P < 0.05$). Numbers represent folds of enrichment (relative quantity) between gene expression in ependymal region and ventral horn.

were considered as consistently expressed in that region (central canal or ventral grey matter). With these genes, we performed statistical comparisons to determine genes enriched in the ependymal region. Enrichment was defined as higher and statistically significant expression in that region versus grey matter (Student's *t*-test of central canal ΔCt versus grey matter ΔCt, $P < 0.05$, with multiple testing correction by Benjamini-Hochberg) (Benjamini *et al.*, 2001; Smyth, 2005). To obtain folds of enrichment, we used relative quantity, $RQ = 2 - \Delta\Delta Ct$, where $\Delta\Delta$Ct for each gene is the difference between the average value of expression in the ependymal region of that gene by the average value of expression of that gene in the grey matter. The quantitative PCR data discussed in this publication have been deposited in NCBI's Gene Expression Omnibus (Edgar *et al.*, 2002), and are accessible through GEO Series accession number GSE65463 (http://www.ncbi.nlm.nih.gov/geo/query/acc.cgi?acc=GSE65463).

Results

MRI shows a generalized absence of central canal in adult humans

Healthy volunteers

We found a generalized absence of patent canal in volunteers of all ages from 18 years on. The qualitative observation showed that the central canal was absent in >70% of spinal cord levels in the majority of the cases, except for two young individuals (55% and 65% of absence), with frequent observation of absence at all spinal cord levels (Fig. 1E). This observation showed no significant correlation with age in the interval studied (Spearman Correlation Test, $P = 0.63$). When studied level by level, central canal patency (either complete or partial) was observed mainly in cervical levels but <25% of individuals showed any type of patency (Fig. 1F). In the rest of the levels, <10% of individuals showed any canal patency. No trend was found related to the sex of the individual.

Quantitative estimation using image analysis showed similar results to those with the subjective scoring of the MRI images (Fig. 1I), i.e. that scores of all volunteers were far lower than the values expected for partially patent canals and patent canals (Fig. 1J). No significant correlation was found with age (Spearman Correlation Test, $P = 0.13$) and no differences were found between sexes (Mann-Whitney U-test, $P = 0.46$). We used a single score for each individual (the median value of the scores obtained for the different spinal cord levels) that was representative of the central canal patency in the whole cord (Supplementary Fig. 2). We chose the median as many individuals present outlier values (dots in Fig. 1K and Supplementary Fig. 2A) for which the median is insensitive.

When studying the spinal cord level by level (Fig. 1K), cervical level C1 showed scores significantly higher than the rest of spinal cord levels (Kruskal-Wallis $P < 0.001$; Dunn post-test $P < 0.001$), but still far from the expected value

for partially patent canals. Interestingly, we also found that levels above C1 (medulla) showed a notably higher frequency of patent canals and, therefore, a higher AUC score than spinal cord levels (Kruskal-Wallis $P < 0.001$; Dunn post-test $P < 0.001$).

Injured patients

With injured patients, we only used the quantitative scoring of canal patency based on AUC. None of the three different scores measured for each patient showed significant increases versus control individuals at any age or post-lesional time; this indicates that neither levels with a lesion nor the proximity to the lesion core increased the patency (Fig. 2F–G). Patients with non-traumatic spinal cord injuries showed similar results (Fig. 2H): no significant differences in patency were found with any of the conditions studied.

Morphological features of adult human ependymal region: presence of perivascular pseudorosettes

As observed with MRI, a central canal is absent in spinal cord tissue sections from adult humans. Rather than a patent canal surrounded by ependymal cells, we found dense accumulations of cells, not enclosing cavities or a lumen (Fig. 3A–E).

Our data show that the adult human spinal cord central canal region displays at least three common characteristics distinct from other species in all the individuals studied: first, a notable gliosis formed by a dense mesh of GFAP$^+$ astrocytic processes that surround and occasionally infiltrate ependymal accumulations (Fig. 3F–G). The gliotic region covers almost the whole dorso-ventral extension of central lamina X and extends laterally up to the limits of this lamina.

A second feature is the presence of protoplasmic cells with eccentric nuclei, associated in groups or chains of variable size and normally surrounded by lax extracellular matrix (Fig. 3H). These cells have been described by other authors as ependymocytes (Alfaro-Cervello *et al.*, 2014), showing multiple cilia and basal bodies, and expression of vimentin. We confirmed these observations: the presence of intercellular junctions, beta-catenin expression among cells, and cells with a number of basal bodies indicative of multiple cilia (Supplementary Fig. 4). These adult human spinal cord ependymocytes also show expression of CD15 and GLAST (now known as SLC1A3) (Supplementary Fig. 4), that, in addition to astrocytes, have been related with radial glia and stem/precursor cell phenotypes and described in subpopulations of rodent and human ependymal cells (Sakakibara *et al.*, 2007; Dromard *et al.*, 2008; Sabourin *et al.*, 2009; Obermair *et al.*, 2010; Garcia-Ovejero *et al.*, 2013).

A third feature is the presence of structures previously described as pseudo-canals (Kasantikul *et al.*, 1979; Milhorat *et al.*, 1994; Hugnot and Franzen, 2011; Alfaro-Cervello *et al.*, 2014), consisting of cells radially oriented around a presumed lumen. A subset of these cells expresses vimentin, and their soma is separated from the alleged lumen by a hypocellular GFAP$^+$ ribbon of astrocyte processes (Fig. 3I). However, we have consistently observed that these formations are indeed not arranged around a lumen, but rather around a blood vessel. The difference is important because radial organization around a vessel, with the characteristics described above, should not warrant the term pseudocanal, but instead perivascular pseudorosette, which is a crucial diagnostic feature for ependymoma (Ellison *et al.*, 2004; Wippold and Perry, 2006; Louis *et al.*, 2007*a*, *b*; Scheithauer *et al.*, 2008). We found this feature in all the individuals: a blood vessel is always found in the middle of the alleged lumen in semi-thin sections (Fig. 3J) and confocal images using endothelial markers, such as the Von Willebrand factor (Fig. 3K–L), fibronectin (Fig. 3M), vimentin (Fig. 3N), and nestin (Fig. 3O). Among all samples analysed (36 pseudorosettes found), only one real pseudocanal was present. The difference with a pseudorosette in cell arrangement can be seen in Fig. 3Q–T: in the pseudocanal, cells surrounding the lumen show beta-catenin-positive intercellular junctions and apical acetyl tubulin-positive cilia (Fig. 3S and T). None of those features are observed in pseudorosettes (Fig. 3Q–R).

To further extend this unexpected observation, we aimed to explore other characteristics of ependymomas in this region. Histopathological features of tumours may include cellular proliferation and microvascular proliferation (an apparent multi-layering of endothelium or glomeruloid vasculature) (Louis *et al.*, 2007*b*; Scheithauer *et al.*, 2008). We found no mitotic figures in the ependymal region of any of our samples, and no cell immunoreactivity against Ki67$^+$, an antigen used to establish proliferative index in tumours (Ritter *et al.*, 1998). Absence of Ki67 staining was not due to our protocol, as the same protocol showed extensive proliferation on tissue samples from glioblastomas and anaplastic astrocytomas, which were used as positive controls (Supplementary Fig. 5). A close examination of toluidine blue-stained semi-thin sections showed no microvascular layering in any slice from any individual.

We found other cell types associated with perivascular pseudorosettes, such as CD45$^+$ and Iba1$^+$ microglial cells (Fig. 3U and V), but no beta III tubulin-positive neuronal cell soma, although neuronal processes were frequently found intermingled with the hypocellular GFAP ribbon (Fig. 3W). Finally, immunoreactivity against CD15 and GLAST was also found in pseudorosettes (Fig. 3P and X). We could not find immunoreactivity against SOX2 or PROM1 (previously known as CD133), although both factors were detected in positive controls (glioblastoma and astrocytoma) (Supplementary Fig. 5).

Our histological study also confirmed that low medulla frequently presents with a patent canal. Of the eight individuals studied, seven showed different degrees of canal patency, and only one presented with an obliterated canal

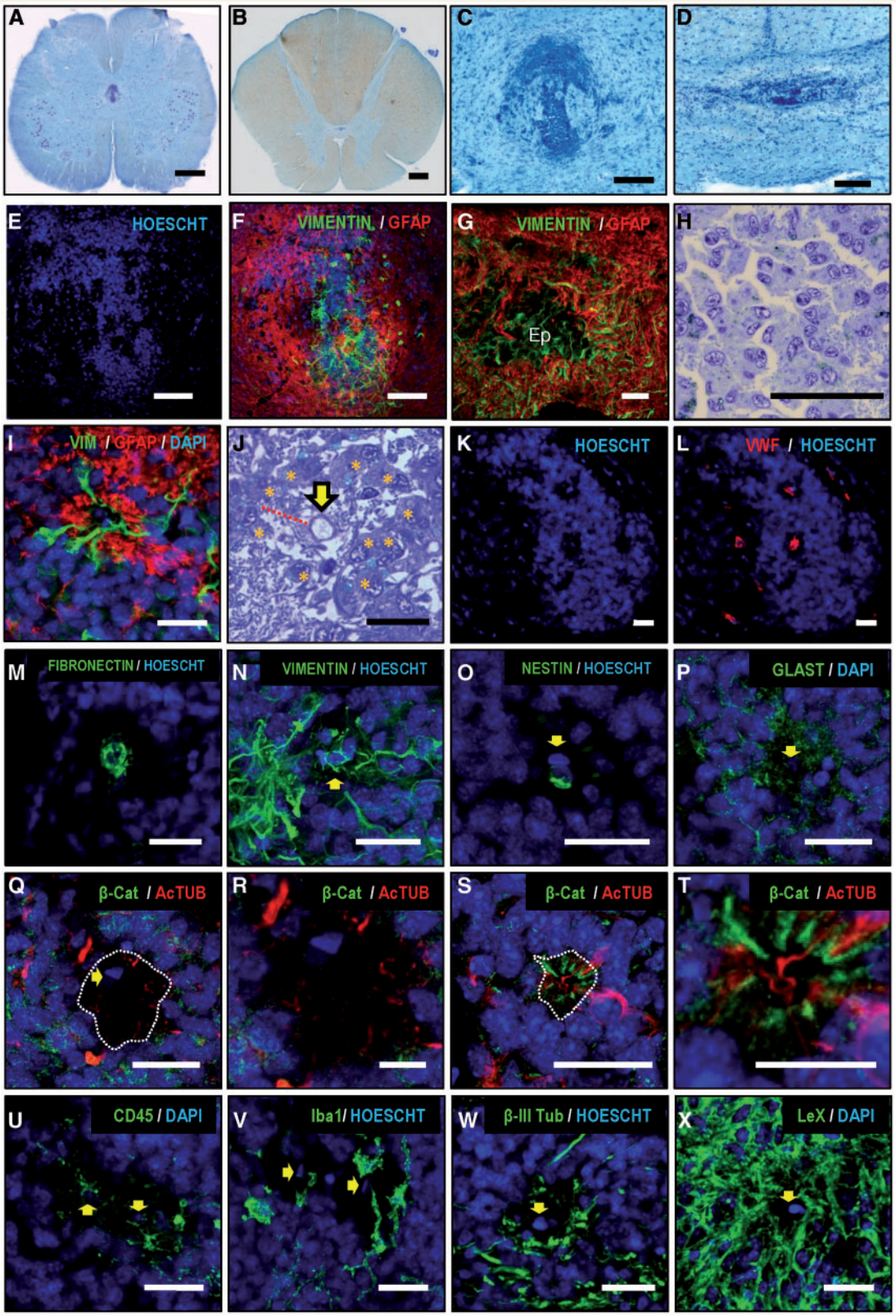

Figure 3 Histological characterization of the adult ependymal region. (**A** and **B**) Macroscopic view of lumbar and thoracic spinal cord levels of two individuals (Nissl staining). (**C** and **D**) Higher magnification details of the ependymal region of pictures **A** and **B**, showing accumulations of cells not enclosing any lumen or patent canal. (**E** and **F**) Confocal images show that those cell accumulations are surrounded by a dense mesh of GFAP processes. (**G**) GFAP$^+$ processes surround and infiltrate the ependymal region (Ep) formed by vimentin-positive cells. (**H**) Cells in the ependymal region frequently appear associated in clusters of several cells with eccentric nuclei and characteristics of ependymocytes. (**I**) In every sample studied, we found structures consisting of cells radially oriented around a presumed lumen separated from it by a hypocellular

(continued)

(Supplementary Fig. 3A–P). In all cases, ependymal alignment around the lumen was observed, as well as an intense GFAP$^+$ astrogliosis around the canal (Supplementary Fig. 3Q–S).

Gene expression of adult human ependymal region

We tested our laser capture microdissection samples against genes described as being overexpressed in ependymomas, particularly in posterior fossa and spinal cord ependymomas, given the differing gene expression profiles of ependymomas from different regions of the CNS (Taylor *et al.*, 2005; Modena *et al.*, 2006; Johnson *et al.*, 2010).

We assessed 117 ependymoma-related genes and found that 96 of them (82.1%) were expressed in the normal adult ependymal region. However, 43 of those genes were equally expressed in cells from the grey matter, unrelated with ependymal cells or ependymoma (Supplementary Table 6). The rest of the 53 genes were significantly enriched in the ependymal region versus grey matter (45.3% total) (Table 4 and Fig. 4B).

Among enriched genes, we found genes prominent in spinal cord ependymomas [*FREM1*, *c9orf24*, *MLC1* and homeobox (Hox) genes] versus other types of ependymomas (Taylor *et al.*, 2005; Modena *et al.*, 2006; Palm *et al.*, 2009). Furthermore, the gene expression profile was compatible with a non-aggressive tumour (Table 4), as was expected after histological observation. There was low or absent expression of genes related to proliferation (*MCM2*, *MKI67*, *PCNA* and *CCND1*) and enrichment in genes related to low grade ependymomas. Witt *et al.* (2011) described two distinct groups of infratentorial ependymomas that can be delimitated by two sets of genes: Group A (tumours found in young individuals, much more likely to exhibit recurrence, metastasis at recurrence, and death), and Group B (older patients, with a lower recurrence and better prognosis). Our gene profile shows an enrichment of normal ependyma in 'Group B' genes (7 of 11 genes: *AGBL2*, *EFHB*, *LINGO2*, *MAL2*, *NELL2*, *ROPN1L*, *TSGA10*), rather than in 'Group A' (1 of 11 genes: RELN). In addition, nestin, which also correlates with ependymoma progression (Milde *et al.*, 2012), is expressed, but not enriched, in the ependymal region. Parker *et al.* (2014) showed that aggressiveness and invasion of ependymomas are correlated with expression of *L1CAM* (not expressed by our samples), *CCND1*, and *RELA* (not enriched in our samples). We also found low levels or absence of other genes related to high grade ependymomas, such as *TNC*, *MFAP5*, and *COL4A1* (Palm *et al.*, 2009; Puget *et al.*, 2009; Andreiuolo *et al.*, 2010; Witt *et al.*, 2011), or genes related to malignancy of tumours, like *PROM1* (Puget *et al.*, 2009; Peyre *et al.*, 2010), which is only expressed at parenchymal levels. Finally, upregulation of several members of the Notch family has consistently been related to ependymomas (*NOTCH1*, *NOTCH2*, *JAG1*, *JAG2*, *HES1*, *HEY2*), and associated with recurrence (Taylor *et al.*, 2005; Modena *et al.*, 2006; Puget *et al.*, 2009). We only found enrichment of *HEY2*, while levels of *NOTCH1*, *NOTCH2*, *JAG1*, and *HES1* were equivalent to normal grey matter (Table 4).

We built a second panel of genes to test whether ependymal region gene expression may be compatible with the expression found in the central canal or spinal cord-derived stem cells from rodents and primates. It must be noted that the molecular distinction of tumours versus stem cell niches is rather blurred because the two conditions share many properties and molecular profiles. Some studies have even defined neural stem cells or radial glia as the origin of ependymoma (Taylor *et al.*, 2005; Modena *et al.*, 2006; Johnson *et al.*, 2010); for instance, Notch signalling is a normal feature of ependymal cells in the brain and spinal cord during development and adulthood and is also activated after damage (Yamamoto *et al.*, 2001; Carlen *et al.*, 2009). Accordingly, at least 34 genes in our list were described in both contexts (ependymoma and rodent/primate central canal cells): *ARHGEF28, BHLHE40, CCND1, CD34, CXCL12, EGFR, FLNB, FOXG1, HES1, HEY1, HEY2, HOXA5, HOXA7, HOXA9, HOXB1, HOXB2, HOXB6, HOXB7, HOXC6, HOXC8, HOXC9, HOXC10, HOXD3, HOXD9, HOXD10, JAG1, MLC1, MSI1, NES, NOTCH1, NOTCH2, NKX6.1, PROM1*, and *SOX11*.

Figure 3 Continued

layer with a GFAP$^+$ ribbon. (**J**) Toluidine blue-stained semi-thin section showing that cells are radially oriented (asterisks) forming a perivascular pseudorosette around a central vessel (yellow arrow). Glial processes form a hypocellular region between the vessel and the cell soma (*red line*). (**K** and **L**) Vessels inside pseudorosettes can be detected with Von Willebrand factor (red) (**L**), fibronectin (**M**), vimentin (**N**) and nestin (**O**). (**P**) GLAST is found in the astrocyte ribbon and in parenchymal cells but not in the central vessel. (**Q**) Differences between perivascular pseudorosettes and pseudocanals can be observed using B-catenin (green) and acetyl-tubulin (red) staining. (**Q**) A perivascular pseudorosette shows absence of cilia (red) oriented to the central vessel and absence of radially oriented β-catenin-positive intercellular junctions (green) in the apical part of the cells. The dashed line depicts the border of the hypocellular layer described in (**I**). The yellow arrow points to endothelial cell nucleus. (**R**) Higher magnification of **Q**. Acetyl-tubulin short processes remain in the hypocellular layer (**S**). A pseudocanal shows radially-oriented cells maintaining cell polarity with apical beta-catenin in the intercellular junctions and cilia oriented towards canal lumen. (**T**) Higher magnification of **S**. (**U**) CD45$^+$ immune cells are found in the perivascular pseudorosette. (**V**) Iba-1$^+$ microglia are frequently related to perivascular pseudorosettes. (**W**) Beta III tubulin-positive neuronal processes but not neuronal somata are found associated with pseudorosettes. (**X**) Perivascular pseudorosettes express high levels of Lewis antigen X (**CD15**). Yellow arrows point to the position of central vessel. Scale bars: **A** and **B** = 1 mm; **C** and **D** = 200 μm; **E** and **F** = 100 μm; **G–I**, **K–Q**, **S**, **U–X** = 25 μm; **J**, **R**, **T** = 10 μm.

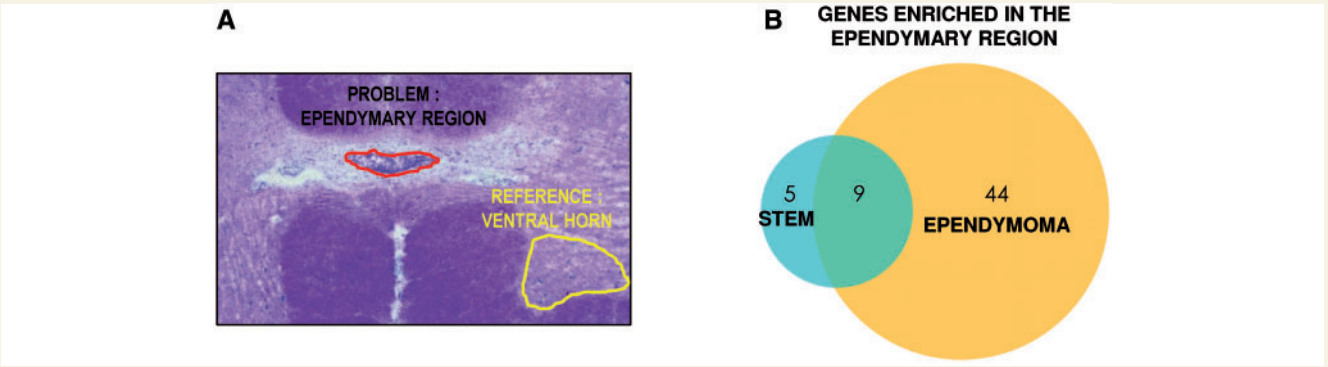

Figure 4 Gene expression profile of ependymal region cells obtained by laser capture microdissection. (**A**) Scheme showing the ependymal region dissected with the laser microscope and a reference region from the ventral horn to establish gene enrichment. (**B**) Venn diagram showing the genes enriched in the ependymal region belonging to stem or ependymoma profiles.

We assessed up to 93 spinal cord neurogenic niche-related genes (including the 34 genes already mentioned) and found that 61 of them (65.6%) were expressed in the normal adult ependymal region. Of these, the level of expression of 47 genes was not significantly different from that found in the ventral horn (Supplementary Table 5). Only 14 of them were enriched in the ependymal region (15.1% total; Table 3): five described only for central canal (*BDNF, CD24, FOXJ1, PAX6, PAX7*) and nine more also described as being expressed by ependymoma (*ARHGEF28, HEY2, HOXA5, HOXA7, HOXC8, HOXC9, HOXC10, MLC1, MSI1*) (Fig. 4B).

Discussion

In the current study, we show that the adult human ependymal region, unlike rodents, lacks a central canal in most spinal cord levels in the vast majority of individuals. There has been previous evidence supporting this finding using histology on post-mortem tissues (Clarke, 1859; Weigert, 1895; Cornil, 1933; Netsky, 1953; Kasantikul *et al.*, 1979; Milhorat *et al.*, 1994; Yasui *et al.*, 1999), but the evidence was generally neglected or, alternatively, interpreted as a post-mortem artefact (Dromard *et al.*, 2008; Hugnot and Franzen, 2011). We demonstrate here that the absence of patency is found in living individuals to the same extent of that described in post-mortem samples (Milhorat *et al.*, 1994; Yasui *et al.*, 1999); this evidence, therefore, eliminates its consideration as a technical artefact. In addition, the use of MRI allowed us to explore the features of the central canal in normal as well as after traumatic and non-traumatic spinal cord injuries, a previously unexplored issue.

The possibility might exist that injury would induce a rearrangement of the ependymal region so that ependymocytes may form new canals. We show here that injuries do not produce such an effect, and there are no notable changes in MRI signal in central grey, independently of the time after lesion, proximity to the injury site, or to the presence of damage at that level. We have not relied on subjective impressions while evaluating MRI data, and have used a quantitative method to support our visual score. In addition, we wanted to rule out the possibility that the absence of patency is a transient effect caused by the pulsatile flow of the CSF (Wagshul *et al.*, 2011). We found two pieces of evidence that argue against this: first, we performed the same MRI experiment in rats, finding, as expected, a generalized patency (Supplementary Fig. 1); second, we did a longitudinal follow-up of some young patients who showed patent canal at some levels at the initial time points, observing a progressive and permanent loss of patency with time (Supplementary Fig. 1).

Further evidence against the obliteration of the central canal as an artefact or a temporal modification is the complex structure that replaces the previous lumen of the canal. Previous authors have described morphological features of this structure, including gliosis, accumulation of cells identified as ependymocytes, and structures that they defined as pseudocanals or rosettes (Kasantikul *et al.*, 1979; Yasui *et al.*, 1999; Hugnot and Franzen, 2011; Alfaro-Cervello *et al.*, 2014). Our findings only partially support those descriptions. Unexpectedly, we have found that the structures described as pseudocanals are instead perivascular pseudorosettes, composed of cells radially arranged around a vessel, not around a lumen. This changed our perspective on the study of this region because perivascular pseudorosettes are a diagnostic feature of ependymoma (Wippold and Perry, 2006; Louis *et al.*, 2007*b*). At first glance, it may seem meaningless to think about the presence of spinal cord tumours in the general population because the incidence of ependymomas is described to be below 0.3 per 100 000 people (Louis *et al.*, 2007*b*). However, histology and the genetic profile consistently support the ependymoma-like nature of the adult ependymal region, although quiescent or belonging to a very low-grade type. As defined by the WHO, ependymomas are the most common neuroepithelial neoplasms, comprising 50–60% of spinal gliomas in adults, although they are less frequent in children (Schiffer, 1997; Auguste and Gupta, 2006) and are

generally slow-growing tumours. What we observe is that a 'normal' profile in humans, at least in adults, may be closer to low-grade ependymomas than to the idea of a 'normal' ependyma based on children or animal models.

The cause of central canal occlusion and the appearance of ependymoma-like structures is currently unknown. Several possible reasons have been hypothesized, such as mechanical damage due to maturation of the cord or viral infections (Kasantikul *et al.*, 1979; Milhorat and Kotzen, 1994; Milhorat *et al.*, 1994; Yasui *et al.*, 1999; Louis *et al.*, 2007*b*). However, it may be speculated that the mechanism of central canal closure and the mechanism that underlies ependymoma formation may be common. In this case, surrounding tissue would be able to control transformation and keep it in a non-reactive state in the majority of the population, whereas in some cases ependymoma may arise. More studies would be needed to unravel this, mostly exploring the age in which the transition from a patent to an occluded canal with pseudorosettes is produced.

This unexpected scenario raises other questions related to cell replacement and neurogenesis: can this region without a patent canal and with an unconventional morphology count as a neurogenic niche? Does it express genes known to be representative of the same structure in rodents and primates? To partially answer these questions, we explored the expression of additional genes normally expressed by the spinal cord central canal niche or derived stem cells from other species. We found enrichment of only 14 genes related to neurogenic niches versus 53 related to ependymoma. Only one group has been able to perform *in vitro* assays with human ependymal cells; they found that human ependymal neurospheres may give rise to cells expressing glial and neuronal markers (GFAP, GABA, 5-HT), but cannot be passaged (Dromard *et al.*, 2008; Hugnot and Franzen, 2011). Moreover, when cultured in adherent conditions, these cells can be passaged, but produce cells with a molecular profile compatible with mesodermal cell types (Mamaeva *et al.*, 2011). Together, the morphological, molecular, and functional data may question the role of adult spinal cord ependyma as a neurogenic niche in adult humans, but more functional studies are needed to fully support this claim.

Another question that may arise is how the absence of a patent canal in SCI patients would fit with the existence of post-traumatic syringomyelia, in which the cyst produced by the lesion expands rostrally and caudally, forming a fluid-filled cavity (syrinx) that affects several spinal levels (Rossier *et al.*, 1985; Brodbelt and Stoodley, 2003). Milhorat *et al.* (1995) described that post-traumatic syrinxes are 'extracanalicular' i.e. cavities located paracentrally in the grey or white matter, which do not involve the enlargement of the central canal. Accordingly, we observe this paracentral location of the syrinx in our axial images of patients with post-traumatic syringomyelia (data not shown). This does not exclude the central canal as a possible origin of post-traumatic syringomyelia, because post-traumatic syringomyelia is developed in only 2–8% of SCI patients (Klekamp *et al.*, 2002; Ko *et al.*, 2012); this is compatible with the extremely low frequency of canal patency that we describe here. However, the paracentral extension of the syrinx and the involvement of many levels argues against central canal dilation as the mechanism of syrinx expansion. Rather, it seems that canal stenosis limits this expansion as proposed (Milhorat *et al.*, 1995). This highlights another important difference with rats, in which an ascending and progressive central canal dilation has been described after a spinal contusion (Radojicic *et al.*, 2007).

Collectively, we show here that the adult human central canal is very different from that of rodents and other primates in structure, cellular composition, and genetic profile. Although the ependymal region does express some genes of stem/precursor cells and holds ependymal cells, our results suggest that the current model for endogenous cell replacement, based on rodents and other primates, should be taken with caution when considering translation to adult humans. On the other hand, it still may apply to children and perhaps to high cervical levels in young individuals who show a higher frequency of canal patency. Our current observations may raise other important questions: how does that arrangement of cells with that molecular profile behave after injury? How does it respond to subsequent pharmacological treatment or cell transplantation? Can this structure be modulated to enhance tissue repair? Does it hold a latent danger of transformation? More studies on human samples or using new experimental models closer to the adult human situation are needed to answer these questions. Such answers would help to further understand and improve manipulation of this niche in order to achieve the final major goal: cell replacement and neural repair.

Acknowledgements

We would like to thank the volunteers that gave us their time and cooperation in undergoing MRI. In particular, we want to thank Antonio G.A. who sadly passed away before seeing this manuscript published. We are grateful to the personnel at the Radiology Service in the HNP (Margarita Velasco, Antonio Martinez, Dionisio Santillana, Celia Gómez) and at the Radiology Department at TCM, who helped with MRI acquisition and data collection. We also thank Javier Mazarío and José Ángel Rodriguez-Alfaro at the Microscopy Facilities at the National Hospital for Paraplegics, Martin Ian Maher at the electron microscopy facilities in the Cajal Institue (Madrid), Concepción Sanchez Caro and Beatriz Navarro Galve for their help. Marien Fernandez, David Castejon, and Palmira Villa (CAI de Resonancia Magnetica, Universidad Complutense de Madrid) provided technical assistance with the rat MRI. Finally, we would also like to thank Dr Helmut Kettenmann who gave us

easy access to many important classic papers from the 19th and 20th centuries in http://www.networkglia.eu/en/classicpapers.

Funding

This work was funded by Wings For Life Foundation. Laboratory of Neuroinflammation has been supported by Instituto de Salud Carlos III (Ministry of Economy and Competitiveness of Spain) and Fundación Mutua-Madrileña (Madrid, Spain).

Supplementary material

Supplementary material is available at *Brain* online.

References

Abematsu M, Tsujimura K, Yamano M, Saito M, Kohno K, Kohyama J, et al. Neurons derived from transplanted neural stem cells restore disrupted neuronal circuitry in a mouse model of spinal cord injury. J Clin Invest 2010; 120: 3255–66.

Alelu-Paz R, Iturrieta-Zuazo I, Byne W, Haroutunian V, Garcia-Villanueva M, Rabano A, et al. A new antigen retrieval technique for human brain tissue. PLoS One 2008; 3: e3378.

Alfaro-Cervello C, Cebrian-Silla A, Soriano-Navarro M, Garcia-Tarraga P, Matias-Guiu J, Gomez-Pinedo U, et al. The adult macaque spinal cord central canal zone contains proliferative cells and closely resembles the human. J Comp Neurol 2014; 522: 1800–17.

Alfaro-Cervello C, Soriano-Navarro M, Mirzadeh Z, Alvarez-Buylla A, Garcia–Verdugo JM. Biciliated ependymal cell proliferation contributes to spinal cord growth. J Comp Neurol 2012; 520: 3528–52.

Andreiuolo F, Puget S, Peyre M, Dantas-Barbosa C, Boddaert N, Philippe C, et al. Neuronal differentiation distinguishes supratentorial and infratentorial childhood ependymomas. Neuro Oncol 2010; 12: 1126–34.

Auguste KI, Gupta N. Pediatric intramedullary spinal cord tumors. Neurosurg Clin N Am 2006; 17: 51–61.

Barnabé-Heider F, Göritz C, Sabelström H, Takebayashi H, Pfrieger FW, Meletis K, et al. Origin of new glial cells in intact and injured adult spinal cord. Cell Stem Cell 2010; 7: 470–82.

Beattie MS. Inflammation and apoptosis: linked therapeutic targets in spinal cord injury. Trends Mol Med 2004; 10: 580–3.

Benjamini Y, Drai D, Elmer G, Kafkafi N, Golani I. Controlling the false discovery rate in behavior genetics research. Behav Brain Res 2001; 125: 279–84.

Brodbelt AR, Stoodley MA. Post-traumatic syringomyelia: a review. J Clin Neurosci 2003; 10: 401–8.

Carlen M, Meletis K, Goritz C, Darsalia V, Evergren E, Tanigaki K, et al. Forebrain ependymal cells are Notch-dependent and generate neuroblasts and astrocytes after stroke. Nat Neurosci 2009; 12: 259–67.

Carro MS, Lim WK, Alvarez MJ, Bollo RJ, Zhao X, Snyder EY, et al. The transcriptional network for mesenchymal transformation of brain tumours. Nature 2010; 463: 318–25.

Ceruti S, Villa G, Genovese T, Mazzon E, Longhi R, Rosa P, et al. The P2Y-like receptor GPR17 as a sensor of damage and a new potential target in spinal cord injury. Brain 2009; 132: 2206–18.

Clarke JL. Further researches on the grey substance of the spinal cord. Philos Trans R Soc Lond 1859; 149: 437–67.

Cornil L, Mosinger M. Sur les processus prolifereratifs de l'ependyme medullaire (Rapports avec les tumeurs intramedullaires et la syringomyelie). Rev Neurol (Paris) 1933; 1: 749–54.

Dromard C, Guillon H, Rigau V, Ripoll C, Sabourin JC, Perrin FE, et al. Adult human spinal cord harbors neural precursor cells that generate neurons and glial cells *in vitro*. J Neurosci Res 2008; 86: 1916–26.

Edgar R, Domrachev M, Lash AE. Gene Expression Omnibus: NCBI gene expression and hybridization array data repository. Nucleic Acids Res 2002; 30: 207–10.

Ellison DL, Love S, Chimelli L, Harding B, Lowe JS, Vinters HV, Brandner S, Yong YH, editor. Neuropathology. A reference text of CNS pathology. 2nd edn. Mosby: Elsevier; 2004.

Fandel D, Wasmuht D, Avila-Martin G, Taylor JS, Galan-Arriero I, Mey J. Spinal cord injury induced changes of nuclear receptors PPARalpha and LXRbeta and modulation with oleic acid/albumin treatment. Brain Res 2013; 1535: 89–105.

Fu H, Qi Y, Tan M, Cai J, Hu X, Liu Z, et al. Molecular mapping of the origin of postnatal spinal cord ependymal cells: Evidence that adult ependymal cells are derived from Nkx6.1+ ventral neural progenitor cells. J Comp Neurol 2003; 456: 237–44.

Garcia-Ovejero D, Arevalo-Martin A, Paniagua-Torija B, Sierra-Palomares Y, Molina-Holgado E. A cell population that strongly expresses the CB1 cannabinoid receptor in the ependyma of the rat spinal cord. J Comp Neurol 2013; 521: 233–51.

Goritz C, Frisen J. Neural stem cells and neurogenesis in the adult. Cell Stem Cell 2012; 10: 657–9.

Horner PJ, Power AE, Kempermann G, Kuhn HG, Palmer TD, Winkler J, et al. Proliferation and differentiation of progenitor cells throughout the intact adult rat spinal cord. J Neurosci 2000; 20: 2218–28.

Hu Z, Zimmermann BG, Zhou H, Wang J, Henson BS, Yu W, et al. Exon-level expression profiling: a comprehensive transcriptome analysis of oral fluids. Clin Chem 2008; 54: 824–32.

Hugnot JP, Franzen R. The spinal cord ependymal region: a stem cell niche in the caudal central nervous system. Front Biosci (Landmark Ed) 2011; 16: 1044–59.

Johansson CB, Momma S, Clarke DL, Risling M, Lendahl U, Frisen J. Identification of a neural stem cell in the adult mammalian central nervous system. Cell 1999; 96: 25–34.

Johnson RA, Wright KD, Poppleton H, Mohankumar KM, Finkelstein D, Pounds SB, et al. Cross-species genomics matches driver mutations and cell compartments to model ependymoma. Nature 2010; 466: 632–6.

Kasantikul V, Netsky MG, James AE Jr. Relation of age and cerebral ventricle size to central canal in man. Morphological analysis. J Neurosurg 1979; 51: 85–93.

Kelly TK, Karsten SL, Geschwind DH, Kornblum HI. Cell lineage and regional identity of cultured spinal cord neural stem cells and comparison to brain-derived neural stem cells. PLoS One 2009; 4: e4213.

Klekamp J, Iaconetta G, Batzdorf U, Samii M. Syringomyelia associated with foramen magnum arachnoiditis. J Neurosurg 2002; 97: 317–22.

Ko HY, Kim W, Kim SY, Shin MJ, Cha YS, Chang JH, et al. Factors associated with early onset post-traumatic syringomyelia. Spinal Cord 2012; 50: 695–8.

Koelliker A. Handbuch der Gewebelehre des Menschen. Nervensystem des Menschen und der Thiere. Leipzig: Engelmann; 1893.

Louis DN, Ohgaki H, Wiestler OD, Cavenee WK, Burger PC, Jouvet A, et al. The 2007 WHO classification of tumours of the central nervous system. Acta Neuropathol 2007a; 114: 97–109.

Louis DNO, Wiestler OD, Cavenee WK, editor. WHO classification of tumours of the central nervous system. 4th edn. Lyon: IARC; 2007b.

Lu P, Woodruff G, Wang Y, Graham L, Hunt M, Wu D, et al. Long-distance axonal growth from human induced pluripotent stem cells after spinal cord injury. Neuron 2014; 83: 789–96.

Mamaeva D, Ripoll C, Bony C, Teigell M, Perrin FE, Rothhut B, et al. Isolation of mineralizing Nestin+ Nkx6.1+ vascular muscular cells from the adult human spinal cord. BMC Neurosci 2011; 12: 99.

Mamber C, Kozareva DA, Kamphuis W, Hol EM. Shades of gray: The delineation of marker expression within the adult rodent subventricular zone. Prog Neurobiol 2013; 111: 1–16.

McDonough A, Martinez-Cerdeno V. Endogenous proliferation after spinal cord injury in animal models. Stem Cells Int 2012; 2012: 387513.

Meletis K, Barnabe-Heider F, Carlen M, Evergren E, Tomilin N, Shupliakov O, et al. Spinal cord injury reveals multilineage differentiation of ependymal cells. PLoS Biol 2008; 6: e182.

Milde T, Hielscher T, Witt H, Kool M, Mack SC, Deubzer HE, et al. Nestin expression identifies ependymoma patients with poor outcome. Brain Pathol 2012; 22: 848–60.

Milhorat TH, Capocelli AL Jr, Anzil AP, Kotzen RM, Milhorat RH. Pathological basis of spinal cord cavitation in syringomyelia: analysis of 105 autopsy cases. J Neurosurg 1995; 82: 802–12.

Milhorat TH, Kotzen RM. Stenosis of the central canal of the spinal cord following inoculation of suckling hamsters with reovirus type I. J Neurosurg 1994; 81: 103–6.

Milhorat TH, Kotzen RM, Anzil AP. Stenosis of central canal of spinal cord in man: incidence and pathological findings in 232 autopsy cases. J Neurosurg 1994; 80: 716–22.

Modena P, Lualdi E, Facchinetti F, Veltman J, Reid JF, Minardi S, et al. Identification of tumor-specific molecular signatures in intracranial ependymoma and association with clinical characteristics. J Clin Oncol 2006; 24: 5223–33.

Namimatsu S, Ghazizadeh M, Sugisaki Y. Reversing the effects of formalin fixation with citraconic anhydride and heat: a universal antigen retrieval method. J Histochem Cytochem 2005; 53: 3–11.

Netsky MG. Syringomyelia; a clinicopathologic study. AMA Arch Neurol Psychiatry 1953; 70: 741–77.

Obermair FJ, Fiorelli R, Schroeter A, Beyeler S, Blatti C, Zoerner B, et al. A novel classification of quiescent and transit amplifying adult neural stem cells by surface and metabolic markers permits a defined simultaneous isolation. Stem Cell Res 2010; 5: 131–43.

Palm T, Figarella-Branger D, Chapon F, Lacroix C, Gray F, Scaravilli F, et al. Expression profiling of ependymomas unravels localization and tumor grade-specific tumorigenesis. Cancer 2009; 115: 3955–68.

Parker M, Mohankumar KM, Punchihewa C, Weinlich R, Dalton JD, Li Y, et al. C11orf95-RELA fusions drive oncogenic NF-kappaB signalling in ependymoma. Nature 2014; 506: 451–5.

Petit A, Sanders AD, Kennedy TE, Tetzlaff W, Glattfelder KJ, Dalley RA, et al. Adult spinal cord radial glia display a unique progenitor phenotype. PLoS One 2011; 6: e24538.

Peyre M, Commo F, Dantas-Barbosa C, Andreiuolo F, Puget S, Lacroix L, et al. Portrait of ependymoma recurrence in children: biomarkers of tumor progression identified by dual-color microarray-based gene expression analysis. PLoS One 2010; 5: e12932.

Pfenninger CV, Steinhoff C, Hertwig F, Nuber UA. Prospectively isolated CD133/CD24-positive ependymal cells from the adult spinal cord and lateral ventricle wall differ in their long-term *in vitro* self-renewal and *in vivo* gene expression. Glia 2011; 59: 68–81.

Puget S, Grill J, Valent A, Bieche I, Dantas-Barbosa C, Kauffmann A, et al. Candidate genes on chromosome 9q33-34 involved in the progression of childhood ependymomas. J Clin Oncol 2009; 27: 1884–92.

R Development Core Team. R: A language and environment for statistical computing. Vienna, Austria: R Foundation for Statistical Computing; 2014.

Radojicic M, Nistor G, Keirstead HS. Ascending central canal dilation and progressive ependymal disruption in a contusion model of rodent chronic spinal cord injury. BMC Neurology 2007; 7: 30.

Ramon y Cajal S. Textura del sistema nervioso del hombre y de los vertebrados. Madrid: Moya; 1899/1904.

Retzius G. Studien über Ependym und Neuroglia. Biologische Untersuchungen 1893; 5: 2–26.

Ritter AM, Hess KR, McLendon RE, Langford LA. Ependymomas: MIB-1 proliferation index and survival. J Neurooncol 1998; 40: 51–7.

Rossier AB, Foo D, Shillito J, Dyro FM. Posttraumatic cervical syringomyelia. Incidence, clinical presentation, electrophysiological studies, syrinx protein and results of conservative and operative treatment. Brain 1985; 108 (Pt 2): 439–61.

Sabelstrom H, Stenudd M, Frisen J. Neural stem cells in the adult spinal cord. Exp Neurol 2014; 260C: 44–9.

Sabourin JC, Ackema KB, Ohayon D, Guichet PO, Perrin FE, Garces A, et al. A Mesenchymal-Like ZEB1+Niche Harbors Dorsal Radial Glial Fibrillary Acidic Protein-Positive Stem Cells in the Spinal Cord. Stem Cells 2009; 27: 2722–33.

Sakakibara A, Aoki E, Hashizume Y, Mori N, Nakayama A. Distribution of nestin and other stem cell-related molecules in developing and diseased human spinal cord. Pathol Int 2007; 57: 358–68.

Scheithauer BW, Fuller GN, VandenBerg SR. The 2007 WHO classification of tumors of the nervous system: controversies in surgical neuropathology. Brain Pathol 2008; 18: 307–16.

Schiffer D. Brain tumours biology, pathology, and clinical references. Berlin: Springer; 1997.

Shihabuddin LS, Ray J, Gage FH. FGF-2 is sufficient to isolate progenitors found in the adult mammalian spinal cord. Exp Neurol 1997; 148: 577–86.

Smyth GK. Limma: linear models for microarray data. In: Gentleman R, Carey V, Dudoit S, Irizarry R, Huber W, editors. . Bioinformatics and computational biology solutions using R and bioconductor. New York: Springer; 2005. p. 397–420.

Taylor MD, Poppleton H, Fuller C, Su X, Liu Y, Jensen P, et al. Radial glia cells are candidate stem cells of ependymoma. Cancer Cell 2005; 8: 323–35.

Tetzlaff W, Okon EB, Karimi-Abdolrezaee S, Hill CE, Sparling JS, Plemel JR, et al. A systematic review of cellular transplantation therapies for spinal cord injury. J Neurotrauma 2011; 28: 1611–82.

Tysseling VM, Mithal D, Sahni V, Birch D, Jung H, Belmadani A, et al. SDF1 in the dorsal corticospinal tract promotes CXCR4+ cell migration after spinal cord injury. J Neuroinflammation 2011; 8: 16.

von Lenhossek M. Der Feinere Bau des Nervenssystems im Lichte neuerer Forschung. Berlin: Gustav Fischer; 1895.

Wagshul ME, Eide PK, Madsen JR. The pulsating brain: A review of experimental and clinical studies of intracranial pulsatility. Fluids Barriers CNS 2011; 8: 5.

Wani K, Armstrong TS, Vera-Bolanos E, Raghunathan A, Ellison D, Gilbertson R, et al. A prognostic gene expression signature in infratentorial ependymoma. Acta Neuropathol 2012; 123: 727–38.

Weigert K. Beiträge zur Kenntnis der normalen menschlichen Neuroglia. Frankfurt: Diesterweg; 1895.

Weiss S, Dunne C, Hewson J, Wohl C, Wheatley M, Peterson AC, et al. Multipotent CNS stem cells are present in the adult mammalian spinal cord and ventricular neuroaxis. J Neurosci 1996; 16: 7599–609.

Wippold FJ 2nd, Perry A. Neuropathology for the neuroradiologist: rosettes and pseudorosettes. AJNR Am J Neuroradiol 2006; 27: 488–92.

Witt H, Mack SC, Ryzhova M, Bender S, Sill M, Isserlin R, et al. Delineation of two clinically and molecularly distinct subgroups of posterior fossa ependymoma. Cancer Cell 2011; 20: 143–57.

Yamamoto S, Nagao M, Sugimori M, Kosako H, Nakatomi H, Yamamoto N, et al. Transcription factor expression and Notch-dependent regulation of neural progenitors in the adult rat spinal cord. J Neurosci 2001; 21: 9814–23.

Yang H. Endogenous Neurogenesis Replaces Oligodendrocytes and Astrocytes after Primate Spinal Cord Injury. Journal of Neuroscience 2006; 26: 2157–66.

Yasui K, Hashizume Y, Yoshida M, Kameyama T, Sobue G. Age-related morphologic changes of the central canal of the human spinal cord. Acta Neuropathol 1999; 97: 253–9.